Ab Initio Characterization of the Isomerism Between the μ-η2:η2-Peroxo- and bis(μ-oxo)dicopper Cores

ARTICLE · JANUARY 1996

CITATION
1

READS
20

3 AUTHORS, INCLUDING:

Christopher J Cramer
University of Minnesota Twin Cities
532 PUBLICATIONS **23,481** CITATIONS

SEE PROFILE

Ab Initio Characterization of the Isomerism between the μ-η^2:η^2-Peroxo- and Bis(μ-oxo)dicopper Cores

Christopher J. Cramer,* Bradley A. Smith, and William B. Tolman*

Contribution from the Department of Chemistry, Center for Metals in Biocatalysis, and Supercomputer Institute, University of Minnesota, 207 Pleasant St. SE, Minneapolis, Minnesota 55455-0431

Received July 17, 1996[⊗]

Abstract: The interconversion of model compounds $\{[(NH_3)_3Cu]_2(\mu\text{-}\eta^2\text{:}\eta^2\text{-}O_2)\}^{2+}$ (**1**) and $\{[(NH_3)_3Cu]_2(\mu\text{-}O)_2\}^{2+}$ (**2**) has been examined using multireference second-order perturbation theory with an 8-electron/8-orbital active space. At this level of theory, **1** and **2** are separated by only 0.3 kcal/mol, and the barrier to isomerization is predicted to be very low based on single-point energy calculations for intermediate structures. The flat nature of the potential energy surface along the interconversion coordinate derives from a balancing of Coulomb forces and nondynamic electron correlation. The latter effect depends critically on the significant energy change experienced by the $13a_u$ σ^*_{OO} virtual orbital on passing from one isomer to the other. In addition, solvation electrostatics favor **2** over **1**.

Introduction

In quest of an understanding of the mechanisms by which dioxygen is activated by copper sites in biological and catalytic systems, significant effort has been expended toward the synthesis, characterization, and study of the reactivity of complexes derived from the reaction of Cu(I) precursors with O_2.[1−4] An important motif in such complexes is the structurally defined $[Cu_2(\mu\text{-}\eta^2\text{:}\eta^2\text{-}O_2)]^{2+}$ core **A**[5] which also is present in oxyhemocyanin and oxytyrosinase.[6,7] Recently, **A** and a new isomeric form in which the O−O bond is cleaved, $[Cu_2(\mu\text{-}O)_2]^{2+}$ (**B**) were characterized in synthetic systems incorporating 1,4,7-triazacyclononane capping ligands.[8−10] Moreover, the ability of cores **A** and **B** to rapidly equilibrate was documented in a novel illustration of reversible O−O bond scission and formation in a bimetallic system.[10]

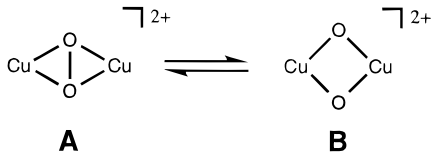

A **B**

Theory has played an important role in efforts to understand the geometric and electronic structures of various metal dioxygen complexes.[11,12] Prior theoretical work on dicopper complexes has focused predominantly on the $[Cu_2(\mu\text{-}\eta^2\text{:}\eta^2\text{-}O_2)]^{2+}$ core;[5,11,13−16] Solomon and co-workers have emphasized in particular the utility of broken-symmetry density functional theory (BS-DFT) calculations in rationalizing the spectroscopic properties of experimentally characterized examples.[6,17,18] For the alternative core, bare $[Cu_2(\mu\text{-}O)_2]^{2+}$ has been characterized at the *restricted* DFT level[19] (which, in contrast to BS-DFT, favors systems having strong metal−metal interactions[20]). In addition, BS-DFT calculations on $\{[(NH_3)_3Cu_2](\mu\text{-}O)_2\}^{2+}$ have been reported to converge to restricted solutions[9] and the conformational and vibrational behavior of this molecule has been examined at the restricted Hartree−Fock (RHF) and multiconfiguration second-order perturbation theory (CASPT2) levels, the latter with a 2-electron/2-orbital active space.[21] Eisenstein et al. have emphasized the importance of including at least two electronic configurations in calculations designed to compare the energies for different copper−peroxo binding motifs (e.g., side-on vs end-on).[16]

In this present work, we employ more complete levels of electronic structure theory to probe the differences between model compounds $\{[(NH_3)_3Cu]_2(\mu\text{-}\eta^2\text{:}\eta^2\text{-}O_2)]^{2+}$ (**1**) and $\{[(NH_3)_3\text{-}Cu]_2(\mu\text{-}O)_2]^{2+}$ (**2**) and also to examine their interconversion. In particular, we calculate multiconfigurational molecular wave functions for **1**, **2**, and intermediates along an interconversion pathway using an 8-electron/8-orbital complete active space

[⊗] Abstract published in *Advance ACS Abstracts,* November 1, 1996.

(1) Karlin, K. D.; Gultneh, Y. *Prog. Inorg. Chem.* **1987**, *35*, 219.
(2) Sorrell, T. N. *Tetrahedron* **1989**, *40*, 3.
(3) Kitajima, N.; Moro-oka, Y. *Chem. Rev.* **1994**, *94*, 737.
(4) Fox, S.; Karlin, K. D. In *Active Oxygen in Biochemistry*; Valentine, J. S., Foote, C. S., Greenberg, A., Liebman, J. F., Eds.; Blackie Academic & Professional, Chapman & Hall: Glasgow, Scotland, 1995; p 188.
(5) Kitajima, N.; Fujisawa, K.; Fujimoto, C.; Moro-oka, Y.; Hashimoto, S.; Kitagawa, T.; Toriumi, K.; Tatsumi, K.; Nakamura, A. *J. Am. Chem. Soc.* **1992**, *114*, 1277.
(6) Solomon, E. I.; Tuczek, F.; Root, D. E.; Brown, C. A. *Chem. Rev.* **1994**, *94*, 827.
(7) Magnus, K. A.; Ton-That, H.; Carpenter, J. E. *Chem. Rev.* **1994**, *94*, 727.
(8) Mahapatra, S.; Halfen, J. A.; Wilkinson, E. C.; Que, L., Jr.; Tolman, W. B. *J. Am. Chem. Soc.* **1994**, *116*, 9785.
(9) Mahapatra, S.; Halfen, J. A.; Wilkinson, E. C.; Pan, G.; Cramer, C. J.; Que, L., Jr.; Tolman, W. B. *J. Am. Chem. Soc.* **1995**, *117*, 8865.
(10) Halfen, J. A.; Mahapatra, S.; Wilkinson, E. C.; Kaderli, S.; Young, V. G.; Que, L., Jr.; Zuberbühler, A. D.; Tolman, W. B. *Science* **1996**, *271*, 1397.
(11) Solomon, E. I.; Baldwin, M. J.; Lowery, M. D. *Chem. Rev.* **1992**, *92*, 521.
(12) Bytheway, I.; Hall, M. B. *Chem. Rev.* **1994**, *94*, 639.
(13) Ross, P. K.; Solomon, E. I. *J. Am. Chem. Soc.* **1991**, *113*, 3246.
(14) Maddaluno, J.; Geissner-Prettre, C. *Inorg. Chem.* **1991**, *30*, 3439.
(15) Bernardi, F.; Bottoni, A.; Casadio, R.; Fariselli, P.; Rigo, A. *Int. J. Quantum Chem.* **1996**, *58*, 109.
(16) Eisenstein, O.; Getlicherman, H.; Giessner-Prettre, C.; Maddaluno, J. *Inorg. Chem.* In press.
(17) Baldwin, M. J.; Ross, P. K.; Pate, J. E.; Tyeklár, Z.; Karlin, K. D.; Solomon, E. I. *J. Am. Chem. Soc.* **1991**, *113*, 8671.
(18) Baldwin, M. J.; Root, D. E.; Pate, J. E.; Fujisawa, K.; Kitajima, N.; Solomon, E. I. *J. Am. Chem. Soc.* **1992**, *114*, 10421.
(19) Wang, L.-S.; Wu, H.; Desai, S. R.; Lou, L. *Phys. Rev. B* **1996**, *53*, 8028.
(20) Lovell, T.; McGrady, J. E.; Stranger, R.; Macgregor, S. *Inorg. Chem.* **1996**, *35*, 3079.
(21) Mahapatra, S.; Halfen, J. A.; Wilkinson, E. C.; Pan, G.; Wang, X.; Young, V. G.; Cramer, C. J.; Que, L., Jr.; Tolman, W. B. *J. Am. Chem. Soc.* In press.

S0002-7863(96)02455-9 CCC: $12.00

(CAS) and further employ multireference second-order perturbation theory to obtain our highest quality relative energies. It is important to emphasize that **1** and **2** serve as *qualitative* models for the previously characterized 1,4,7-triazacyclononane capped inorganic systems.[8−10] Thus, our intent is not to provide an extremely accurate potential energy surface for the interconversion of **1** and **2**, but rather to use these calculations to understand certain fundamental aspects of the interconversion that should be transferable to the experimental systems. So, for instance, we will take advantage of X-ray structural data available from the 1,4,7-triazacyclononane capped model systems to validate using very modest levels of electronic structure theory to generate molecular geometries. But, we will use higher levels of theory to provide insights into the electronic structure of these compounds that are not readily available from experiment.

Theoretical Methods

The structures of **1** and **2** were fully optimized within the constraints of C_{2h} symmetry at the RHF level using the STO-3G basis set.[22,23] While this level of theory is clearly not appropriate for energetic comparisons, RHF calculations have been established to give reasonable geometries for closely related complexes by comparison to X-ray crystal structures and/or more complete levels of theory.[9,14,16,21] Given the gas-phase nature of the calculations and the approximations being made for the ligand environment, we consider the additional computational effort that would be required for higher level optimizations to be unwarranted. In addition, the RHF level provides one-electron orbitals of well-defined energy, which will prove useful in the discussion below.

Structures along a model reaction path interconverting **1** and **2** were generated by simultaneously constraining their Cu−Cu and O−O bond lengths according to

$$r_{X-X} = r_{X-X}(\mathbf{1}) + n[r_{X-X}(\mathbf{2}) - r_{X-X}(\mathbf{1})], \quad X = Cu, O;\ n = 0, 0.1, 0.2, ..., 1 \quad (1)$$

and fully relaxing all other degrees of freedom. Two points along this path, structures **3** and **4**, were selected for additional study at higher levels of theory as described below. Structure **4** is in fact the fully optimized transition state structure (one imaginary frequency) for the interconversion of **1** and **2** at the RHF/STO-3G level of theory.

CAS calculations[24] for **1**−**4** were performed using the polarized valence double-ζ (DZP) basis set of Schafer et al.[25] with an 8-electron/8-orbital active space consisting of the $22a_g$, $11b_g$, $21b_u$, $12a_u$, $12b_g$, $13a_u$, $23a_g$, and $22b_u$ orbitals (visualizations of these orbitals are provided as Supporting Information). These orbitals were chosen by examination of orbital occupation numbers from CAS calculations using a variety of different large active spaces for all eight possible singlet and triplet electronic states within C_{2h} symmetry. The final (8,8) space was constructed by inclusion of all CAS orbitals having occupation numbers from 0.01 to 1.99 for **1** and/or **2** in any surveyed electronic state. CASPT2 calculations[26] were carried out using the CAS(8,8) wave function as a reference.

Unpolarized electrostatic components of the solvation free energies, G_P, were calculated for **1** and **2** using the generalized Born equation[27−30]

$$G_P = -\frac{1}{2}\left(1 - \frac{1}{\epsilon}\right)\sum_{k,k'} q_k\, q_{k'}\, \gamma_{kk'} \quad (2)$$

with the dielectric constant ϵ set equal to 10. The summation in eq 2 runs over atoms, the q_k are partial atomic charges, and $\gamma_{kk'}$ is a Coulomb integral dependent on the atomic radii of atoms k and k'.[30] Partial charges were determined from fitting to electrostatic potentials[31] calculated at the Hartree−Fock and density functional levels with the STO-3G basis set—for the latter level of theory both the Xα[32] and BLYP[33,34] functionals were used. For **1**, the DFT electrostatic potentials were derived from broken-symmetry calculations (restricted DFT calculations failed to converge). The atomic radii for H, N, and O were taken from Solvation Model 2,[35] and the atomic radius for Cu was chosen to be 2.1 Å.

HF and DFT calculations, CAS and CASPT2 calculations, and solvation free energy calculations were carried out with the Gaussian 94,[36] MOLCAS,[37] and AMSOL[38] program suites, respectively.

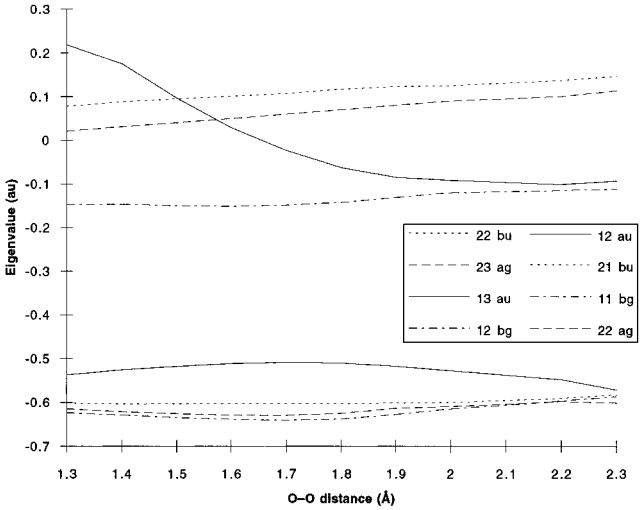

Figure 1. Active space orbital energies at the RHF/STO-3G level along the isomerization coordinate. See Supporting Information for visualizations of these orbitals for **1** and **2**.

Results and Discussion

Figure 1 provides a Walsh diagram of RHF orbital energy eigenvalues for the eight orbitals (four occupied, four virtual) which define the active space in the CAS and CASPT2 calculations. These orbitals were calculated for optimized structures connecting **1** and **2** along a putative reaction coordinate where the Cu−Cu and O−O interatomic distances were constrained to be linearly transformed as described above. Figure 1 illustrates that the isomerization process is not unlike

(22) Hehre, W. H.; Stewart, R. F.; Pople, J. A. *J. Chem. Phys.* **1969**, *51*, 2657.
(23) Hehre, W. J.; Ditchfield, R.; Stewart, R. F.; Pople, J. A. *J. Chem. Phys.* **1970**, *52*, 2769.
(24) Roos, B. O.; Taylor, P. R.; Siegbahn, P. E. M. *Chem. Phys.* **1980**, *48*, 157.
(25) Schafer, A.; Horn, H.; Ahlrichs, R. *J. Chem. Phys.* **1992**, *97*, 2571.
(26) Andersson, K.; Malmqvist, P.-Å.; Roos, B. O.; Sadlej, A. J.; Wolinski, K. *J. Phys. Chem.* **1990**, *94*, 5483.
(27) Hoijtink, G. J.; de Boer, E.; Van der Meij, P. H.; Weijland, W. P. *Recl. Trav. Chim. Pays-Bas* **1956**, *75*, 487.
(28) Jano, I. *C. R. Acad. Sci. Paris* **1965**, *261*, 103.
(29) Still, W. C.; Tempczyk, A.; Hawley, R. C.; Hendrickson, T. *J. Am. Chem. Soc.* **1990**, *112*, 6127.
(30) Cramer, C. J.; Truhlar, D. G. *J. Am. Chem. Soc.* **1991**, *113*, 8305.
(31) Singh, U. C.; Kollman, P. A. *J. Comp. Chem.* **1984**, *5*, 129.
(32) Slater, J. C. *Phys. Rev.* **1951**, *81*, 385.
(33) Becke, A. *J. Chem. Phys.* **1986**, *84*, 4524.
(34) Lee, C.; Yang, W.; Parr, R. G. *Phys. Rev. B* **1988**, *37*, 785.
(35) Cramer, C. J.; Truhlar, D. G. *Science* **1992**, *256*, 213.
(36) Frisch, M. J.; Trucks, G. W.; Schlegel, H. B.; Gill, P. M. W.; Johnson, B. G.; Robb, M. A.; Cheeseman, J. R.; Keith, T.; Petersson, G. A.; Montgomery, J. A.; Raghavachari, K.; Al-Laham, M. A.; Zakrzewski, V. G.; Ortiz, J. V.; Foresman, J. B.; Cioslowski, J.; Stefanov, B. B.; Nanayakkara, A.; Challacombe, M.; Peng, C. Y.; Ayala, P. Y.; Chen, W.; Wong, M. W.; Andres, J. L.; Replogle, E. S.; Gomperts, R.; Martin, R. L.; Fox, D. J.; Binkley, J. S.; Defrees, D. J.; Baker, J.; Stewart, J. P.; Head-Gordon, M.; Gonzalez, C.; Pople, J. A. *Gaussian 94 RevD.1*; Gaussian Inc.: Pittsburgh, PA, 1995.
(37) Andersson, K.; Blomberg, M. R. A.; Fülscher, M. P.; Karlström, G.; Kellö, V.; Lindh, R.; Malmqvist, P.-Å.; Noga, J.; Olsen, J.; Roos, B. O.; Sadlej, A. J.; Siegbahn, P. E. M.; Urban, M.; Widmark, P.-O. *MOLCAS-3*; University of Lund: Sweden, 1994.
(38) Hawkins, G. D.; Lynch, G. C.; Giesen, D. J.; Rossi, I.; Storer, J. W.; Liotard, D. A.; Cramer, C. J.; Truhlar, D. G. *QCPE Bull.* **1996**, *16*, 11.

Table 1. Core Interatomic Distances and Relative Energies for the ^1A_g States of **1**−**4**[a]

structure	*r*CuCu, Å	*r*OO, Å	relative energy (kcal/mol) CASPT2(8,8)/DZP
1	3.758	1.324	0.0[b]
3	3.400[c]	1.600[c]	−5.8
4[d]	3.004	1.796	−1.3
2	2.734	2.281	0.3

[a] Structures optimized at RHF/STO-3G level. [b] Absolute energy (hartrees): −3765.239 60. [c] Constrained bond length. [d] Transition state structure at the RHF/STO-3G level.

a symmetry-allowed pericyclic reaction,[39] with a continuous diabatic correlation of occupied orbitals along the entire reaction path.

Table 1 lists the relative energies of **1** and **2** calculated at the CAS and CASPT2 levels of theory. Energies for two additional structures that are roughly equally spaced along the linear reaction coordinate, **3** and **4**, are also reported. At the RHF/STO-3G level, **4** is the transition state (TS) structure for the interconversion of **1** and **2** (one imaginary frequency with appropriate eigenvector), but the position of this TS would likely change significantly were electron correlation effects to be included.

All energies are calculated for the ^1A_g singlet states. Solomon has used a valence bond configuration interaction analysis to assign the ground state of **1** as ^1A_g lying 2480 cm^{-1} below the ^3B_u triplet (i.e., $-2J^{GS} = -2480$ cm^{-1}).[40] With BS-DFT at the BLYP/STO-3G level, assuming a singlet/triplet weighting in the BS-DFT energy proportional to $\langle S^2 \rangle$ for the Kohn−Sham determinant,[41] we calculate a similar splitting of 2880 cm^{-1}. This same level of theory predicts the ^1A_g−^3B_u splitting in **2** to be 2250 cm^{-1} (without any need for a BS description of the singlet). These results are entirely consistent with the observed diamagnetism for both isomeric forms in the analogous experimental systems.

At our highest level of theory, namely CASPT2(8,8)/DZP, **1** is found to be more stable than **2** by only 0.3 kcal/mol. Intervening structures **3** and **4** are slightly lower in energy than either end point at this level, implying either that the RHF geometries for these structures are closer to the true CASPT2 geometries than is the case for **1** and **2** or possibly that for this system in the gas phase there is only a single minimum energy structure that is intermediate between **1** and **2**. However, given the large number of degrees of freedom for these systems and the lack of available analytic gradients, it is not practical to attempt further geometric refinements at the CASPT2 level. Moreover, it is not really **1** and **2** that are of interest, but rather what these results tell us about larger analogs. The important implication for the experimentally characterized systems, which have structures in good correspondence with those found for **1** and **2**, is that the *intrinsic* barrier to interconversion, i.e., absent counterions, condensed-phase effects, ligand strain, etc., must be very low. We did not examine DFT calculations for this reaction coordinate because of the ambiguities associated with determining the relative weights of singlet and triplet contributions to the BS-DFT densities in the absence of spectroscopic data for comparison.[41−43]

The flat nature of the potential energy surface along this coordinate derives from a remarkable cancellation of two competing effects. Coulomb forces favor **1** over **2** because of the greater separation of the positively charged metal centers. In the naive approximation of unit charges at each copper atom with all other atoms uncharged and a vacuum dielectric constant, the magnitude of this effect would be about 33 kcal/mol. Stabilizing **2**, however, is an interesting non-dynamic electron correlation effect, arising from the significant lowering in energy of the $13a_u$ virtual orbital (Figure 1). This orbital includes some O−O σ^* character in **1**, and is correspondingly high in energy—indeed, the energetic cost of that σ^* interaction is so high that the $13a_u$ orbital in **1** is actually dominated by copper 4p contributions (Figure 2). However, as the O−O bond breaks on going from **1** to **2**, the O−O σ^* interaction becomes much less unfavorable until ultimately in **2** the $13a_u$ virtual orbital contains roughly equal contributions from the O−O σ^* and copper 3d orbitals and ends up close in energy to the $12b_g$ LUMO.

The presence of this additional low-lying virtual orbital in **2** compared to **1** stabilizes **2**, as configurations with this orbital populated now make larger contributions to the CAS wave function (i.e., non-dynamic correlation). In a physical sense, this formal mixing of ground- and excited-state *configurations* of similar energy may be regarded as the wave function equivalent of hyperconjugation, which is a stabilizing effect that derives from the mixing of filled and empty *orbitals* of similar energy. The relative importance of this effect may be ascertained from inspection of the CAS wave functions for **1**−**4**; Table 2 lists configurations contributing at least 2%. It is noteworthy that **1** is very well described (>98%) by a simple 2-configuration wave function mixing the reference configuration $|...11b_g^2 22a_g^2 21b_u^2 12a_u^2\rangle$ with the configuration derived from exciting both electrons in the $12a_u$ HOMO into the $12b_g$ LUMO. Compound **2**, on the other hand, includes four other configurations with weights above 2%, and derives about an additional 15% total from configurations having weights below 2%. One critical aspect of this multiconfigurational stabilization is that the $13a_u$ virtual orbital that is so much lower in energy for **2** than for **1** is of the same symmetry as the $12a_u$ HOMO. Thus, single excitations with appropriate spin coupling, which are less energetically costly than double excitations over the same gap, can contribute to the ^1A_g ground state wave function.

Proserpio et al.[44] have discussed the analogous participation of the O−O σ^* orbital in the reaction coordinate for the isomerization of $\{[(H_2O)_4Mn]_2(\mu\text{-}\eta^2\text{:}\eta^2\text{-}O_2)\}^{4+}$ to $\{[(H_2O)_4Mn]_2(\mu\text{-}O)_2\}^{4+}$. In contrast to the dicopper system, where, as described above, the two dioxygen binding motifs are very close in energy, they find this isomerization to be exoergic by 5 eV at the extended Hückel level. Moreover, at this level of theory that process is predicted to be barrierless, i.e., only the $\{[(H_2O)_4Mn]_2(\mu\text{-}O)_2\}^{4+}$ isomer is stable. It is not clear how much of the difference between the copper and manganese models may be ascribed to the quantitative unreliability of extended Hückel theory. We note in this regard that the simple RHF/STO-3G level predicts isomerization of **1** to **2** to be endoergic by 72.6 kcal/mol, suggesting that the errors at single-determinantal levels of theory can be very large indeed.

Although experiment makes clear that appropriately substituted $[Cu_2(\mu\text{-}\eta^2\text{:}\eta^2\text{-}O_2)]^{2+}$ and $[Cu_2(\mu\text{-}O)_2]^{2+}$ cores can be in equilibrium in solution, it is entirely fortuitous that the energetic separation between analogs **1** and **2** is predicted to be so close to zero at the CASPT2 level. One important effect not present in the gas-phase calculations is the effect of solvation on the experimental equilibrium. Given the significant difference in

(39) Woodward, R. B.; Hoffmann, R. *Conservation of Orbital Symmetry*; Academic Press: New York, 1970.
(40) Tuczek, F.; Solomon, E. I. *J. Am. Chem. Soc.* **1994**, *116*, 6916.
(41) Noodleman, L.; Case, D. A. *Adv. Inorg. Chem.* **1992**, *38*, 423.
(42) Ziegler, T.; Rauk, A.; Baerends, E. J. *Theor. Chim. Acta* **1977**, *43*, 261.
(43) Cramer, C. J.; Dulles, F. J.; Giesen, D. J.; Almlöf, J. *Chem. Phys. Lett.* **1995**, *245*, 165.
(44) Proserpio, D. M.; Hoffmann, R.; Dismukes, G. C. *J. Am. Chem. Soc.* **1992**, *114*, 4374.

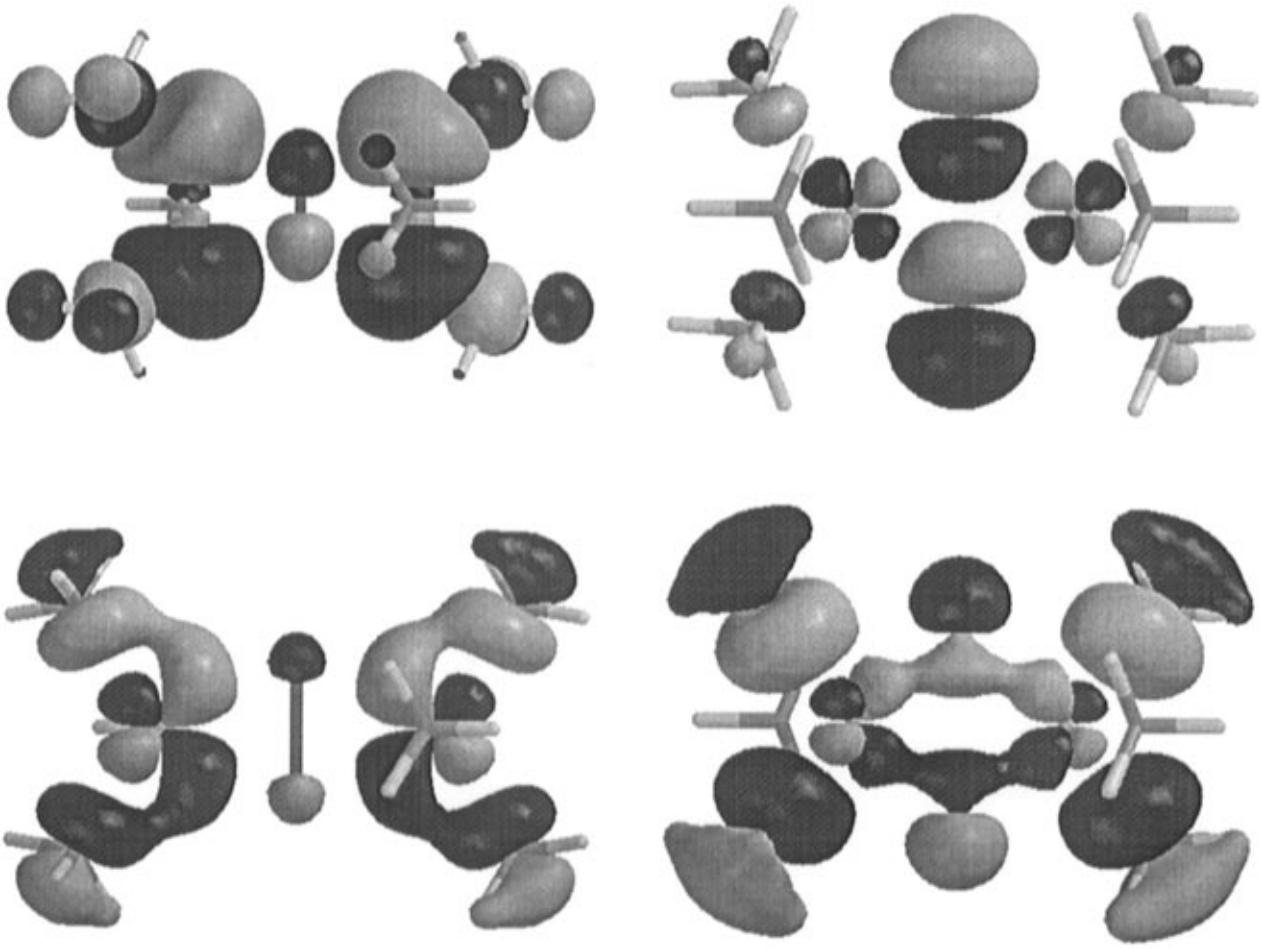

Figure 2. Visualization of the 0.032 au isodensity surfaces for the $12a_u$ (lower) and $13a_u$ (upper) orbitals in **1** (left) and **2** (right).

Table 2. Configuration Weights in the CAS(8,8)/DZP Wave Functions for **1**−**4**

	occupation no.								
structure	$22a_g$	$11b_g$	$21b_u$	$12a_u$	$12b_g$	$13a_u$	$23a_g$	$22b_u$	wt, %
1	2	2	2	2	0	0	0	0	64.9
	2	2	2	0	2	0	0	0	33.3
3	2	2	2	2	0	0	0	0	62.5
	2	2	2	0	2	0	0	0	36.1
4	2	2	2	2	0	0	0	0	57.9
	2	$\underline{2}$	2	0	$\underline{2}$	0	0	0	15.5
	2	$\underline{1}$	2	1	$\underline{1}$	$\underline{1}$	0	0	5.4
	2	1	2	1	$\underline{1}$	$\underline{1}$	0	0	4.7
	0	2	2	2	2	0	0	0	3.6
2	2	$\underline{2}$	2	2	$\underline{0}$	0	0	0	63.0
	2	$\underline{1}$	2	1	$\underline{1}$	1	0	0	7.6
	2	2	2	0	2	0	0	0	4.8
	2	2	2	0	$\underline{0}$	$\underline{2}$	0	0	3.9
	1	2	1	2	$\underline{1}$	$\underline{1}$	0	0	3.6
	2	1	2	1	$\underline{1}$	$\underline{1}$	0	0	2.4

Coulomb energies noted above for these dicationic cores, condensed phase effects may be expected to be significant. To estimate the influence of a surrounding dielectric medium on this equilibrium, we have carried out continuum dielectric calculations within a generalized Born formalism. Table 3 contains copper and oxygen atomic partial charges calculated from fitting to electrostatic potentials calculated at the RHF, Xα, and BLYP levels of theory. The solvation free energies are calculated for a dielectric medium characterized by $\epsilon = 10$. Although there is considerable variation between the RHF and DFT charges, the net solvation free energies are largely unaffected. At all levels of theory we find **2** to be better solvated than **1** by 5.6 to 8.4 kcal/mol. Structures **3** and **4** had solvation free energies intermediate between **1** and **2**, i.e., solvation does not have any special effect on the reaction barrier. While these calculations predict the differential electrostatic effect of bulk solvent, they do *not* account for possible differences in the specific interactions of **1** and **2** with the first solvation shell, which may be very important. Moreover, differential solvation will be reduced with increasingly bulky ligands, since the ligand volume will descreen the core charges. Nevertheless, the generalized Born model provides an indication of how the equilibrium will shift in response to changes in the dielectric constant of the solvent absent specific interactions.

Table 3. Copper and Oxygen Partial Atomic Charges and Solvation Free Energies for **1** and **2**

theory[a]	structure[b]	q_{Cu}, au[c]	q_O, au[c]	G_P, kcal/mol[d]	rel G_P, kcal/mol
RHF	**1**	0.23	−0.10	−141.5	0.0
	2	0.43	−0.42	−149.9	−8.4
Xα	**1**	0.02	−0.08	−144.9	0.0
	2	−0.06	−0.14	−151.8	−6.9
BLYP	**1**	0.10	−0.11	−142.9	0.0
	2	0.02	−0.16	−148.5	−5.6

[a] All calculations use the STO-3G basis set. [b] RHF/STO-3G optimized structures. [c] From fitting to the electrostatic potential. [d] See eq 2.

Finally, we note for the CASPT2 calculations described above that the weight of the CAS reference wave function in the second-order perturbation theory expansion is about 66% for **1**, **2**, **3**, and **4**. This consistency across structures lends confidence in the validity of the results given the single electronic state involved in the interconversion of **1** and **2** (i.e., the ^1A_g state). However, we found very poor agreement

between CASPT2 predicted excited-state energies[45] and observed ultraviolet absorptions.[10] There are several possible explanations for this discrepancy. Compounds **1** and **2** may be inappropriate models for the spectroscopy of more complex systems, medium/counterion effects may have a significant effect on the spectra, and/or the CAS active space may still be inadequate for these calculations. Calibrated DFT calculations thus appear to offer a more economical method for providing insight into the electronic spectroscopy of $[Cu_2(\mu\text{-}O)_2]^{2+}$ cores; we note in particular the good performance of BS-DFT methods for $[Cu_2(\mu\text{-}\eta^2\text{:}\eta^2\text{-}O_2)]^{2+}$ cores[6,11,13,18,46] and of restricted DFT methods for multiplet splittings in systems where broken-symmetry techniques are not required.[47−50]

Conclusions

High-level multiconfigurational ab initio theory predicts that model compounds $\{[(NH_3)_3Cu]_2(\mu\text{-}\eta^2\text{:}\eta^2\text{-}O_2)\}^{2+}$ and $\{[(NH_3)_3Cu]_2(\mu\text{-}O)_2\}^{2+}$ are very nearly equal in energy and that the energetic barrier to their interconversion, if one exists, is small. Electrostatic interactions favor the peroxo isomer over the bis-oxo isomer but solvation reduces this effect. The bis-oxo isomer is strongly stabilized by non-dynamic electron correlation relative to the peroxo isomer because a virtual orbital dominated by O−O σ* character lies at much lower energy in the former system than is found for the latter.

Acknowledgment. We are grateful for high-performance vector and parallel computing resources made available by the Minnesota Supercomputer Institute and the University of Minnesota-IBM Shared Research Project, respectively. This work was supported by NSF (CHE-9525819) and NIH (GM47365).

Supporting Information Available: Pseudo-three-dimensional color pictures of the RHF/STO-3G orbitals corresponding to the (8,8) active space in the CAS calculations are available on the ACS Web site. See any current masthead page for ordering and Internet access instructions.

JA962455N

(45) Cramer, C. J. Unpublished calculations.
(46) Solomon, E. I.; Lowery, M. D. *Science* **1993**, *259*, 1575.
(47) Cramer, C. J.; Dulles, F. J.; Falvey, D. E. *J. Am. Chem. Soc.* **1994**, *116*, 9787.
(48) Cramer, C. J.; Worthington, S. E. *J. Phys. Chem.* **1995**, *99*, 1462.
(49) Lim, M. H.; Worthington, S. E.; Dulles, F. J.; Cramer, C. J. In *Density-Functional Methods in Chemistry*; ACS Symposium Series #629; Laird, B. B., Ross, R. B., Ziegler, T., Eds.; American Chemical Society: Washington, DC, 1996; p 402.
(50) Smith, B. A.; Cramer, C. J. *J. Am. Chem. Soc.* **1996**, *118*, 5490.